

What can quasi-periodic oscillations tell us about the structure of the corresponding compact objects?

George Pappas^{1*}

¹*Section of Astrophysics, Astronomy, and Mechanics, Department of Physics, University of Athens, Panepistimiopolis Zografos GR15783, Athens, Greece*

Accepted 2012 February 23. Received 2012 February 22; in original form 2011 December 21

ABSTRACT

We show how one can estimate the multipole moments of the space-time, assuming that the quasi-periodic modulations of the X-ray flux (quasi-periodic oscillations), observed from accreting neutron stars or black holes, are due to orbital and precession frequencies (relativistic precession model). The precession frequencies Ω_ρ and Ω_z can be expressed as expansions on the orbital frequency Ω , in which the moments enter the coefficients in a prescribed form. Thus, observations can be fitted to these expressions in order to evaluate the moments. If the compact object is a neutron star, constraints can be imposed on the equation of state. The same analysis can be used for black holes as a test for the validity of the no-hair theorem. Alternatively, instead of fitting for the moments, observations can be matched to frequencies calculated from analytic models that are produced so as to correspond to realistic neutron stars described by various equations of state. Observations can thus be used to constrain the equation of state and possibly other physical parameters (mass, rotation, quadrupole, etc.) Some distinctive features of the frequencies, which become evident by using the analytic models, are discussed.

Key words: equation of state – gravitation – methods: analytical – stars: neutron – X-rays: binaries.

1 INTRODUCTION

Low mass X-ray binaries (LMXBs) open a window to some extreme physics. On the one hand the accretion in these systems takes place in the region around a compact object (such as a black hole or a neutron star) where there are strong gravity effects. On the other hand, when the accretion takes place around a neutron star, the properties of the orbital motion depend on the structure of the neutron star itself. Thus studying these systems could provide insight on the properties of gravity in regions where it is yet untested and at the same time help us explore the properties of matter in such extreme conditions as the ones in the interior of neutron stars.

One of the properties that LMXBs often display, are quasi-periodic oscillations (QPOs) in their X-ray flux. This variability appears in a variety of behaviors and is usually organized in various groupings, such as the high-frequency phenomena, the hectohertz QPOs, or the low-frequency complex. The aforementioned categorization is based not only on the frequency range but also on the characteristics

that the observed frequencies display which depend on the type and the state of the source. For example one can observe, (i) in the low-frequency complex low-frequency QPOs with ν values in the range of 0.01 up to 100 Hz or (ii) in the case of high-frequency phenomena, neutron star kHz QPOs (often observed in pairs), called twin kHz QPOs, which have been observed up to $\nu = 1258$ Hz (Jonker et al. (2007)). On the other hand there are high-frequency QPOs which are categorized as black hole high-frequency QPOs and appear to be different than their neutron star counterparts. Finally, the QPOs, apart from the previously mentioned differentiation exhibit also correlations between the various frequency components, both in neutron stars as well as in black holes (for a review see Lamb (2003); van der Klis (2006)).

To explain the QPOs, various types of mechanisms have been proposed. These are: (i) the Beat-frequency models, where one assumes that there is some “beating” of an orbital frequency by the spin frequency of the central object, (ii) the relativistic precession models, where the QPOs are associated with the orbital motion and the periastron or nodal precession of a particular orbit, (iii) the relativistic resonance models, where a type of resonance between the orbital and the epicyclic frequencies is assumed wherever

* E-mail: gpappas@phys.uoa.gr

they have simple integer ratios, and finally (iv) the preferred radii models, where some mechanism chooses a particular radius. These models generally assume the geodesic or almost geodesic orbits of the fluid elements in the accretion disc to be the source of the observed frequencies (see e.g. van der Klis (2006)), while there are also models in which the frequencies are produced from oscillatory modes of the entire disc (see e.g. Rezzolla et al. (1995)). In one way or another all of these models use the properties of the orbits around the compact object onto which the accretion takes place. In our discussion we will refer to the models that assume that the QPOs are caused by the frequencies associated with the orbital motion of the material in the accretion disc such as the relativistic precession models (see Stella (2001)), but our analysis has relevance to the other models as well.

In the relativistic precession models it is assumed that there is some structure or inhomogeneity in the accretion disc (i.e. a hot blob) that follows a keplerian or geodesic orbit which is almost circular and almost at the equatorial plane. Such an orbit has an orbital frequency Ω and precession frequencies, Ω_ρ of radial perturbations and Ω_z of azimuthal (vertical) perturbations. We note here that in the following, while we will assume that such a structure is incorporated in an accretion disc, the orbit of the structure is such that it can be considered to be geodesic, i.e. all forces other than gravity can be ignored. This can be considered to be a good approximation in the case of radiatively efficient thin discs.

The most commonly used assumption for describing the aforementioned frequencies is that the background space-time is either Schwarzschild or Kerr or that it is well approximated by one or the other. A more general assumption for the background space-time would be to assume a stationary and axisymmetric space-time as the one given by the Papapetrou (1953) line element,

$$ds^2 = -f(dt - \omega d\phi)^2 + f^{-1} [e^{2\gamma} (d\rho^2 + dz^2) + \rho^2 d\phi^2]. \quad (1)$$

Such a space-time can be described with the help of the Ernst potential (Ernst (1968a,b)) and the metric functions can be associated to the multipole moments defined by Geroch (1970); Hansen (1974) and Fodor, Honselaers & Perjés (1989). Thus one can express the rotational and epicyclic frequencies as functions of the multipole moments of the space-time. In particular, it was demonstrated by Ryan (1995) that the quantities Ω_ρ/Ω and Ω_z/Ω can be expressed as series expansions on Ω where the coefficients depend on the multipole moments of the underlying space-time. Although Ryan's work was intended to be applied on the analysis of gravitational waves from the adiabatic inspiral of a compact object onto a super-massive central object (extreme mass ratio inspirals, EMRIs), the same principle can be applied in the case of X-ray observations from accretion discs (in LMXBs), assuming that the orbits in the disc are almost circular and almost equatorial.

The expressions given by Ryan are asymptotic expansions that do not give a very good description for the regions close to the innermost stable circular orbit (ISCO). In that case, one could make use of the several proposed analytic space-times that give a faithful description of the geometry around neutron stars (see Stute & Camenzind (2002); Berti & Stergioulas (2004); Pachón, Rueda & Sanabria-Gomez (2006); Pappas (2009);

Teichmüller, Fröb & Maucher (2011)) and use them to work in the strong gravity region. These analytic solutions are constructed by using the first few multipole moments of the space-time which are associated to the properties of the compact object. Thus the assumption of such solutions could relate the frequencies of the QPOs, to the moments of the compact object and give a more accurate description for the QPOs than the typically used geometries of Schwarzschild and Kerr. In our analysis, we will use the two-soliton analytic solution (see Manko, Martín & Ruiz (1995); Pappas (2009)) which is constructed from the first four multipole moments of the neutron star, i.e., the mass (M), the angular momentum (J), the mass quadrupole (M_2) and the spin octupole (S_3).

The benefit of this approach is that instead of relying on gravitational waves (that are at the moment eluding us) to get information for the central compact object, one can rely on electromagnetic observations which are currently abundant. Thus, an algorithm that would produce estimates for the multipole moments of the space-time in low mass X-ray binaries could be used to probe either the equation of state for neutron stars or the no-hair theorem for black holes. Following this point of view, there is currently a programme put forward by Psaltis (2008) on testing gravity with observations in the electromagnetic spectrum.

Our aim in this work is to demonstrate how one could estimate the first few space-time moments by using the series expansions of the frequencies (presented in section 2) and fitting them to QPOs (in section 4). We also present templates for the relation between the various frequencies (in section 5), which are constructed with the help of an analytic solution of the Einstein field equations which has been chosen appropriately so as to describe faithfully the geometry around neutron stars built from realistic EOSs (briefly presented in section 3). Using these templates we show how one could constrain the EOS for matter of higher than nuclear densities that exists inside neutron stars (section 6).

2 THE FREQUENCIES AS FUNCTIONS OF THE MULTIPOLE MOMENTS

In this section we will briefly present the expressions that describe the orbital motion of a test particle in an axisymmetric space-time near the equatorial plane and outline the algorithm that associates the precession frequencies with the orbital frequency and the multipole moments as it was developed by Ryan (1995).

A stationary and axisymmetric space-time can generally be written in the form of the Papapetrou line element given in Eq. (1), where f , ω and γ are functions of the Weyl-Papapetrou coordinates (ρ, z) . In that case, the metric components are:

$$g_{tt} = -f, \quad g_{t\phi} = f\omega, \quad g_{\phi\phi} = f^{-1}\rho^2 - f\omega^2,$$

$$g_{\rho\rho} = g_{zz} = f^{-1}e^{2\gamma},$$

where the radial coordinate is defined as $\rho^2 = g_{t\phi}^2 - g_{tt}g_{\phi\phi}$. The orbit of a particle is usually calculated from the conservation of energy, the conservation of the z component of the angular momentum (where z is the direction of the symmetry axis) and the normalization of the four-velocity. Thus, the two conservation equations are:

$$\frac{E}{\mu} = -g_{tt} \left(\frac{dt}{d\tau} \right) - g_{t\phi} \left(\frac{d\phi}{d\tau} \right), \quad (2)$$

$$\frac{L_z}{\mu} = g_{t\phi} \left(\frac{dt}{d\tau} \right) + g_{\phi\phi} \left(\frac{d\phi}{d\tau} \right), \quad (3)$$

while the normalization of the four-velocity gives:

$$\begin{aligned} -1 &= g_{tt} \left(\frac{dt}{d\tau} \right)^2 + 2g_{t\phi} \left(\frac{dt}{d\tau} \right) \left(\frac{d\phi}{d\tau} \right) \\ &\quad + g_{\phi\phi} \left(\frac{d\phi}{d\tau} \right)^2 + g_{\rho\rho} \left(\frac{d\rho}{d\tau} \right)^2 + g_{zz} \left(\frac{dz}{d\tau} \right)^2. \end{aligned} \quad (4)$$

If the orbit of the particle is on the equatorial plane, then one could define an effective potential from the equation

$$-g_{\rho\rho} \left(\frac{d\rho}{d\tau} \right)^2 = 1 - \frac{\tilde{E}^2 g_{\phi\phi} + 2\tilde{E}\tilde{L}_z g_{t\phi} + \tilde{L}_z^2 g_{tt}}{\rho^2} \equiv V(\rho), \quad (5)$$

where \tilde{E} and \tilde{L}_z are the conserved energy and angular momentum per unit rest mass, respectively, and $V(\rho)$ is the effective potential. From this equation one sees that the conditions for circular orbits are, $d\rho/d\tau = 0$ and $d^2\rho/d\tau^2 = 0$, which are equivalent to the conditions for a local minimum of the effective potential: $V(\rho) = 0$, $dV(\rho)/d\rho = 0$. For the circular motion, one can also derive the orbital frequency,

$$\Omega \equiv \frac{d\phi}{dt} = \frac{-g_{t\phi,\rho} + \sqrt{(g_{t\phi,\rho})^2 - g_{tt,\rho}g_{\phi\phi,\rho}}}{g_{\phi\phi,\rho}}. \quad (6)$$

In case the orbit is not exactly circular or not exactly on the equatorial plane, one can use expressions (2-4) to derive the equation for the perturbed circular motion and from these the epicyclic or precession frequencies Ω_ρ and Ω_z . The expression for the frequencies is

$$\begin{aligned} \Omega_\alpha &= \Omega - \left[-\frac{g^{\alpha\alpha}}{2} \left((g_{tt} + g_{t\phi}\Omega)^2 \left(\frac{g_{\phi\phi}}{\rho^2} \right)_{,\alpha\alpha} \right. \right. \\ &\quad \left. \left. - 2(g_{tt} + g_{t\phi}\Omega)(g_{t\phi} + g_{\phi\phi}\Omega) \left(\frac{g_{t\phi}}{\rho^2} \right)_{,\alpha\alpha} \right. \right. \\ &\quad \left. \left. + (g_{t\phi} + g_{\phi\phi}\Omega)^2 \left(\frac{g_{tt}}{\rho^2} \right)_{,\alpha\alpha} \right) \right]^{1/2}, \end{aligned} \quad (7)$$

where if we set $\alpha \rightarrow \rho$, we obtain the periastron precession and if we set $\alpha \rightarrow z$, we get the nodal precession. Thus, we have the expressions for the orbital frequency and the precession frequencies of an almost circular and almost equatorial orbit.

These expressions depend on the metric functions and their first and second derivatives with respect to the coordinates ρ and z , evaluated on the equatorial plane. As described in Ryan (1995), these functions can be expressed as power series in $1/\rho$. So, by replacing these expressions in the definition of the orbital frequency we obtain

$$\Omega = (M/\rho^3)^{1/2} (1 + \text{series in } \rho^{-1/2}). \quad (8)$$

This series can be inverted to take the form

$$1/\rho = (\Omega^2/M)^{1/3} (1 + \text{series in } \Omega^{1/3}). \quad (9)$$

If we use the above expression to eliminate the $1/\rho$ dependence of the precession frequencies, we end up with a

series with respect to $v = (M\Omega)^{1/3}$ (where, in the Newtonian limit, v is the particle's orbital velocity),

$$\frac{\Omega_\rho}{\Omega} = \sum_{n=2}^{\infty} R_n v^n \quad (10)$$

$$\frac{\Omega_z}{\Omega} = \sum_{n=3}^{\infty} Z_n v^n. \quad (11)$$

The coefficients of the series, R_n and Z_n , depend on the Geroch-Hansen-Fodor multipole moments of the space-time. For example, the first few non-vanishing coefficients are

$$R_2 = 3, \quad R_3 = -4 \frac{S_1}{M^2}, \quad R_4 = \left(\frac{9}{2} - \frac{3M_2}{2M^3} \right), \dots$$

$$Z_3 = 2 \frac{S_1}{M^2}, \quad Z_4 = \frac{3M_2}{2M^3}, \quad Z_6 = \left(7 \frac{S_1^2}{M^4} + 3 \frac{M_2}{M^3} \right), \dots$$

where M and M_2 are the mass and the quadrupole moment, respectively, and S_1 is the angular momentum. These expressions extended up to terms of $O(v^{10})$ can be found in Ryan (1995).

We should point out that in our analysis we are using the term ‘‘frequency’’ for the Ω values which are actually angular velocities while in the literature the observations of QPOs are given as ‘‘cycles/time’’ (ν values). The two are related as $\Omega = 2\pi\nu$. Whenever we refer to the ν frequencies it will be clearly stated so. All quantities are calculated in geometric units (km) except for the frequencies which are usually given in kHz. The conversion from km^{-1} to kHz is performed by multiplying by 299.79, i.e. $1 \text{ km}^{-1} = 299.79 \text{ kHz}$. In these units 1 solar mass (M_\odot) is 1.477 km.

3 THE SPACE-TIME AROUND NEUTRON STARS

In this section we will present the method that we have used to model the space-time around neutron stars. First we briefly discuss the procedure used for generating analytic space-times and then we talk about the choice of specific neutron star models.

3.1 The analytic space-time

As we have said previously, a stationary and axially symmetric space-time can be described by the line element (1). In that case the Einstein field equations in vacuum reduce to the Ernst equation (see Ernst (1968a)),

$$Re(\mathcal{E})\nabla^2\mathcal{E} = \nabla\mathcal{E} \cdot \nabla\mathcal{E}, \quad (12)$$

where the Ernst potential \mathcal{E} , is a complex function of the metric functions.

A general procedure for generating solutions of the Ernst equation has been developed by Sibgatulin (1991); Manko & Sibgatulin (1993); Ruiz, Manko & Martin (1995) and Manko, Martin & Ruiz (1995). The solution of the Ernst equation is produced from a choice of the Ernst potential along the axis of symmetry of the form

$$\mathcal{E}(\rho = 0, z) = e(z) = \frac{P(z)}{R(z)}, \quad (13)$$

where the functions $P(z), R(z)$ are polynomials of order n with complex coefficients in general. In Ruiz et al. (1995), one can find a detailed description of the procedure for generating the solutions by using the parameters of the polynomials in the Ernst potential. It is shown in Ruiz et al. (1995) that the metric functions are finally expressed in terms of some determinants.

The vacuum two-soliton solution (constructed by Manko, Martin & Ruiz (1995)) is a special case of the previous general axisymmetric solution that is obtained from the ansatz (see also Sotiriou & Pappas (2005))

$$e(z) = \frac{(z - M - ia)(z + ib) - k}{(z + M - ia)(z + ib) - k}, \quad (14)$$

where all the parameters are real, while the parameters M and a are the mass and the reduced angular momentum J/M respectively. For this analytic solution, the first five mass and mass-current moments of the corresponding space-time are

$$\begin{aligned} M_0 &= M, & M_1 &= 0, & M_2 &= -(a^2 - k)M, & M_3 &= 0, \\ M_4 &= \left(a^4 - (3a^2 - 2ab + b^2)k + k^2 + \frac{1}{7}(2a^2 - k)M^2 \right) M \\ S_0 &= 0, & J &= aM, & S_2 &= 0, \\ S_3 &= -(a^3 - (2a - b)k)M, & S_4 &= 0. \end{aligned} \quad (15)$$

As it can be seen, the first four moments are linearly related to the parameters of the Ernst potential and thus if they are specified, one can generate an analytic space-time with exactly these first four moments. Specifically, the parameter k is uniquely fixed by the quadrupole M_2 and the parameter b is uniquely fixed by the spin octupole S_3 , while M and a are the mass and the angular momentum per mass, respectively.

The two-soliton solution has been thoroughly studied and has been shown to be a faithful description of the exterior of neutron stars and captures all the characteristics of the corresponding numerical space-times (see Pappas (2009), and for more details ?).

3.2 Neutron star models

In order to construct the analytic space-time exterior to a compact object, one has to choose the appropriate multipole moments. For neutron stars, these moments can be read from numerical models constructed by assuming realistic equations of state. There are several schemes developed for numerically integrating stellar models (see Stergioulas & Friedman (1995), and for an extended list of numerical schemes see Stergioulas (2003)). We have used Stergioulas's RNS code for the construction of the models.

The parameters used to construct the analytic space-time models, i.e., M , a , k and b , are evaluated from the first four multipole moments (M , J , M_2 , S_3) as given by equations (15). In order to cover more space on the "neutron-star parameter space", these moments are obtained from numerically calculated neutron stars with EOSs of varying stiffness. For that purpose we have chosen AU as a typical soft EOS, FPS as a representative moderate stiff EOS and L to describe stiff EOS. After the numerical models are computed, the multipole moments are evaluated according to the algorithm described in Pappas & Apostolatos (2012) since there is a systematic discrepancy in the methods used up to now in the literature.

Table 1. Frequencies calculated for the models constructed with the L EOS. The mass and the radii (circumferential radii at the equator and at ISCO) are given in km. The frequencies are given in kHz. The frequencies are computed at the ISCO except for the cases that the ISCO falls below the surface of the star; then the corresponding frequencies are computed on the surface and are indicated by an asterisk. We note that the frequencies shown are angular frequencies, i.e. $\Omega = 2\pi\nu$.

M (km)	j	R_s (km)	R_{isco} (km)	Ω (kHz)	Ω_ρ (kHz)	Ω_z (kHz)
2.080	0.	14.96	12.48	7.47*	4.42*	0*
2.071	0.194	15.18	11.76	7.26*	3.78*	0.062*
2.075	0.324	15.61	11.98	7.00*	3.47*	0.026*
2.080	0.417	16.06	12.32	6.74*	3.25*	-0.019*
2.083	0.483	16.49	12.63	6.51*	3.06*	-0.054*
2.087	0.543	16.97	12.94	6.26*	2.87*	-0.085*
2.090	0.598	17.51	13.23	5.99*	2.66*	-0.108*
2.095	0.650	18.18	13.53	5.68*	2.42*	-0.122*
2.096	0.690	18.90	13.77	5.37*	2.18*	-0.125*
2.097	0.698	19.09	13.82	5.29*	2.12*	-0.124*
3.995	0.	13.72	23.97	5.10	5.10	0
4.012	0.178	14.23	21.83	5.81	5.81	0.144
4.029	0.280	14.69	20.78	6.24	6.24	0.240
4.051	0.375	15.24	19.98	6.62	6.62	0.327
4.074	0.458	15.87	19.45	6.91	6.91	0.390
4.098	0.528	16.53	19.14	7.11	7.11	0.426
4.120	0.588	17.24	18.99	7.24	7.24	0.438
4.139	0.635	17.95	18.95	7.30	7.30	0.434
4.160	0.682	18.93	18.98	7.34	7.34	0.417
4.167	0.700	19.45	19.01	7.35	7.35	0.407
4.321	0.478	14.90	19.77	6.89	6.89	0.496
4.321	0.479	15.01	19.80	6.88	6.88	0.490
4.324	0.483	15.16	19.80	6.88	6.88	0.489
4.325	0.489	15.29	19.79	6.89	6.89	0.490
4.333	0.505	15.55	19.73	6.93	6.93	0.498
4.355	0.555	16.29	19.53	7.07	7.07	0.525
4.377	0.602	16.99	19.40	7.18	7.18	0.541
4.396	0.641	17.68	19.35	7.25	7.25	0.544
4.418	0.684	18.67	19.35	7.30	7.30	0.535
4.420	0.686	18.74	19.36	7.30	7.30	0.534

For the specifics of the various models chosen, we have followed Berti & Stergioulas (2004). Thus, we have constructed the same constant rest-mass sequences as the ones presented in Berti & Stergioulas (2004) for the corresponding equations of state. That is, every sequence is comprised of models with the same baryon number but different rotation. Specifically for every equation of state, 3 sequences of 10 models with varying rotations are constructed, which correspond to:

- (i) a sequence terminating to a neutron star of $1.4M_\odot$ in the non-rotating limit,
- (ii) a sequence terminating at the maximum-mass neutron star in the non-rotating limit,
- (iii) a supermassive sequence that does not terminate at a non-rotating model.

All the sequences end at the mass-shedding limit on the side of fast rotation, i.e., at the limit where the angular velocity of a particle at the equator is equal to the Keplerian velocity at that radius. These sequences are the so called

Table 2. Fitting results for FPS EOS. The relative differences between the fitted moments and the actual moments of the space-time used are given as a percentage.

M (km)	j	Ω : 1-3 kHz			Ω : 0.3-3 kHz			Ω : 0.1-3 kHz		
		$\frac{\Delta M}{M}$ (per cent)	$\frac{\Delta J}{J}$ (per cent)	$\frac{\Delta M_2}{M_2}$ (per cent)	$\frac{\Delta M}{M}$ (per cent)	$\frac{\Delta J}{J}$ (per cent)	$\frac{\Delta M_2}{M_2}$ (per cent)	$\frac{\Delta M}{M}$ (per cent)	$\frac{\Delta J}{J}$ (per cent)	$\frac{\Delta M_2}{M_2}$ (per cent)
2.067	0.	0.777	-	-	0.211	-	-	0.1025	-	-
2.071	0.201	0.431	14.63	154.3	0.103	4.228	54.34	0.0564	2.562	36.38
2.077	0.301	0.285	6.650	47.46	0.074	2.058	17.50	0.0390	1.191	11.20
2.083	0.385	0.269	4.914	26.95	0.067	1.434	9.310	0.0339	0.804	5.750
2.087	0.452	0.253	3.923	18.01	0.059	1.070	5.753	0.0289	0.576	3.388
2.093	0.507	0.236	3.278	13.26	0.051	0.830	3.872	0.0242	0.424	2.141
2.098	0.557	0.219	2.777	10.10	0.044	0.641	2.625	0.0196	0.305	1.317
2.102	0.603	0.260	3.020	9.940	0.053	0.707	2.590	0.0241	0.340	1.300
2.106	0.636	0.301	3.275	9.995	0.047	0.585	1.957	0.0201	0.262	0.876
2.109	0.666	0.285	2.968	8.561	0.041	0.479	1.452	0.0163	0.194	0.538
2.658	0.	2.236	-	-	0.587	-	-	0.3116	-	-
2.664	0.163	1.277	48.71	1314.	0.306	14.07	463.3	0.1537	7.982	295.4
2.674	0.260	0.723	17.67	285.5	0.185	5.359	104.2	0.0867	2.853	62.76
2.686	0.349	0.479	8.802	99.28	0.133	2.838	37.66	0.0585	1.415	21.26
2.701	0.436	0.358	5.231	43.28	0.069	1.192	11.70	0.0339	0.639	6.825
2.714	0.500	0.329	4.124	27.50	0.055	0.801	6.068	0.0248	0.384	3.029
2.727	0.562	0.237	2.643	14.56	0.039	0.477	2.593	0.0144	0.171	0.701
2.736	0.602	0.214	2.185	10.47	0.028	0.285	0.977	0.0069	0.044	0.373
2.744	0.633	0.194	1.859	7.961	0.019	0.148	0.005	0.0008	0.047	1.023
2.750	0.654	0.179	1.641	6.454	0.012	0.056	0.590	0.0035	0.108	1.409
2.823	0.427	0.351	5.143	56.62	0.066	1.146	14.91	0.0322	0.606	8.542
2.823	0.428	0.439	6.348	67.69	0.089	1.528	19.39	0.0455	0.849	11.73
2.825	0.432	0.350	5.064	52.94	0.066	1.119	13.80	0.0318	0.589	7.859
2.826	0.439	0.348	4.942	49.69	0.064	1.077	12.73	0.0309	0.561	7.159
2.829	0.450	0.343	4.754	45.45	0.062	1.010	11.28	0.0295	0.518	6.204
2.840	0.492	0.322	4.027	31.97	0.052	0.749	6.659	0.0228	0.346	3.137
2.856	0.552	0.231	2.551	16.16	0.036	0.419	2.439	0.0119	0.127	0.338
2.871	0.609	0.195	1.895	9.463	0.018	0.139	0.140	0.0002	0.059	1.356
2.882	0.647	0.116	0.996	3.692	0.007	0.174	2.234	0.0141	0.247	2.650
2.884	0.658	0.108	0.893	2.977	0.010	0.218	2.478	0.0164	0.276	2.799

evolutionary sequences in the sense that an isolated neutron star (i.e. with constant number of baryons) that is losing angular momentum will evolve along such a sequence. In the case that there is accretion onto the neutron star, the baryon number is not constant and the exact evolution of the neutron star depends on several parameters. For a LMXB though, where the mass of the companion is $< 1M_{\odot}$, the overall mass transfer is probably a small fraction of a solar mass and thus a neutron star (with mass $\geq 1.4M_{\odot}$) would evolve following approximately such a sequence. The choice of these particular sequences was made so that the parameter space of the equilibrium neutron star models would be fully sampled (for details on neutron star models and the evolutionary sequences, see Cook, Shapiro & Teukolsky (1994)).

Once all the necessary parameters are at hand the various frequencies can be easily calculated. As an example, we present in Table 1 the radii of the ISCO, the orbital frequency Ω and the two precession frequencies Ω_{ρ} and Ω_z at that radius, for the 3 sequences constructed with L EOS. We also present the masses, the spin parameters ($j = J/M^2$) and the surface radii of the corresponding models. In some models the surface of the star overcomes the radius of the marginally stable orbit and in these cases the respective fre-

quencies are computed on the radius of the surface. One notices that the periastron precession frequency Ω_{ρ} coincides with the orbital frequency Ω at the ISCO and that for the non-rotating models, the nodal precession frequency Ω_z is zero, as expected. The ISCO radii are calculated from the analytic metric, i.e., the two-soliton metric, and thus deviate from the ones given by Stergioulas’s code by at most 3 per cent (Pappas (2009); ?).

4 FITTING THE FREQUENCIES USING THE ASYMPTOTIC EXPRESSIONS

In several occasions, there have been observed twin kHz QPOs with the upper QPO being in a relatively low frequency range (see eg. Boutloukos et al. (2006)) and could thus be considered to come from a region of the accretion disc further than the ISCO (depending on the mass of the central object). In these cases one could directly apply the asymptotic expression presented by Ryan and try to fit for the multipole moments.

In order to explore whether this method could provide useful measurements of the first moments, we will use simulated data [pairs of (Ω, Ω_{ρ})] for the “observed” frequencies of QPOs constructed by assuming the two-soliton analytic

solution. For every numerical model of those discussed in the previous section with multipole moments M , J , M_2 , S_3 , a corresponding two-soliton space-time is constructed and the orbital and precession frequencies for various radii are calculated. From these frequencies, we select the (Ω, Ω_ρ) pairs and plot the ratio Ω_ρ/Ω as a function of Ω . We then fit these data with the expression (10) and calculate the coefficients. From these coefficients, the fitted moments are calculated and compared to the ones used initially to construct the two-soliton space-time.

For the fits we will use data points which correspond to orbital frequencies lower than 3 kHz, which depending on the specifics of the model (mass, rotation and higher moments) correspond to distances greater than $1.4\text{--}2.5 R_{\text{isco}}$. Specifically we will use three frequency ranges for the fits, i.e., from 3 kHz down to 1 kHz (which is between $1.4\text{--}5 R_{\text{isco}}$ depending on the model), $3\text{--}0.3$ kHz ($1.4\text{--}10 R_{\text{isco}}$) and $3\text{--}0.1$ kHz ($1.4\text{--}20 R_{\text{isco}}$). As it will be discussed in the following, the fit in the moments improves as we increase the frequency range, so these ranges have been chosen to demonstrate that effect.

QPOs are observed in the spectrum of X-ray photons in the range of 2–60 keV (see e.g. van der Klis (2006); Lamb (2003)), i.e., within a couple of orders of magnitude in energy. Generally in an accretion disc, the temperature of the disc decreases with the distance as $\propto (r/R_{\text{isco}})^{-3/4}$ (see e.g. Krolik (1999)) which means that in the range between $\sim (1 - 20) R_{\text{isco}}$ there would be a decrease in emitted photons energy of an order of magnitude. Thus, although the $20 R_{\text{isco}}$ is not a limiting distance in any sense for the disc or the QPOs, it is a reasonable choice for a final fitting range for our purpose.

The results of the fits for the models that are based on the FPS EOS are presented in Table 2. These results are typical for all three EOSs. One sees from Table 2 that in the range of frequencies between 1 and 3 kHz (which correspond to distances up to $5R_{\text{isco}}$), the mass can be very accurately constrained. The same applies for the angular momentum for most of the models and especially for those with faster rotation. The quadrupole is generally not very well constrained but for the cases of fast rotation, one could have accuracies better than 30 per cent. As the fitting range increases, the accuracy of the fits improves and becomes quite good for the quadrupole as well. One should also note that the accuracy of a fit deteriorates with increasing mass. That is because the higher the mass of the model, the closer we get to the ISCO for the selected frequency ranges.

5 FITTING THE FREQUENCIES BY USING TEMPLATES

Since Ryan’s expressions are asymptotic expansions in $v = (M\Omega)^{1/3}$, one should not expect them to be very precise in giving the relationship between the frequencies in the region of the space-time near the marginally stable orbit, which corresponds to Ω frequencies, greater than about 3–4 kHz. For this reason, it would be useful to have templates of frequencies, for different models constructed with different EOSs, on which to project the observations. In this section we will present such templates using the three EOSs that we have already discussed.

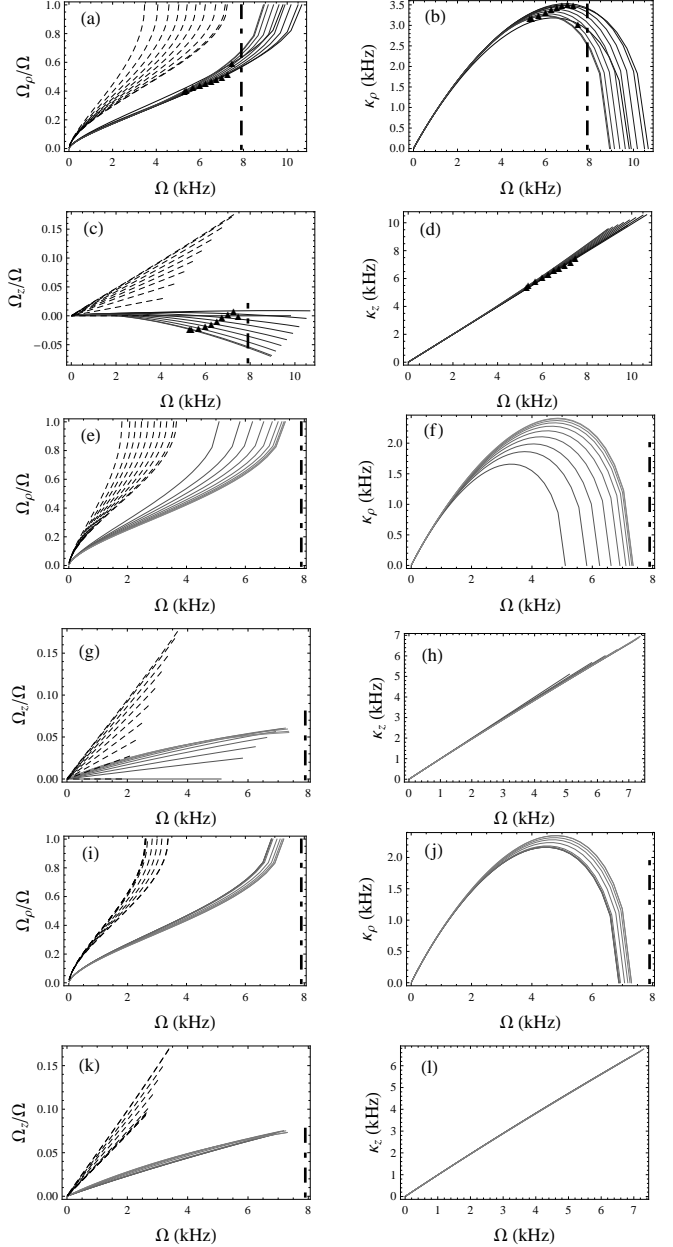


Figure 1. Plot of frequencies for the three sequences of models for the L EOS. Plots (a–d) are for sequence (i), (e–h) are for sequence (ii) and (i–l) are for sequence (iii). All curves are terminated at the ISCO. The black triangles represent the surface of the neutron star for the particular model, if the ISCO is under the surface. The dashed lines correspond to the frequencies for Kerr space-times of the same mass and rotation parameter as the corresponding neutron star models. The dashed-dotted line denotes the maximum QPO frequency measured up to now.

For every EOS, we produce by means of the two-soliton metric, the three frequencies Ω , Ω_ρ and Ω_z and the two oscillation frequencies, $\kappa_\rho = \Omega - \Omega_\rho$ for the radial perturbation and $\kappa_z = \Omega - \Omega_z$ for the vertical perturbation. The precession frequencies, actually the ratios Ω_ρ/Ω , Ω_z/Ω , and oscillation frequencies are plotted against the orbital frequency Ω for the three sequences of neutron star models. In Fig.

1 we present the plots for the L EOS. The behavior of the frequencies is similar for all the equations of state.

As it can be seen from the templates, in the case of the orbital frequency and the periastron precession frequency, as the orbit approaches the marginally stable orbit the two frequencies become equal. That is to be expected, since the precession frequency is the difference between the orbital frequency and the frequency of the radial perturbation, which goes to zero at the ISCO (the change of sign from positive to negative of the square of the frequency of the radial perturbation marks the onset of the radial instability). That could be used as a criterion of whether a pair of observed kHz QPOs are the orbital and the precession frequencies or not. If they are, then one would expect that the evolution of the two frequencies should bring them together on the ISCO before they disappear.

Another important feature that arises is that the precession frequencies behave differently than the corresponding Kerr frequencies. More specifically, in some cases the nodal precession at high orbital frequencies (which correspond to the inner part of the disc near the marginally stable orbit) becomes zero. That is because the vertical perturbation of the orbit has a frequency equal to the orbital one. That never happens in the Kerr geometry (see Fig. 1) and the effect is due to the difference between the multipole moments of a realistic neutron star and those of the Kerr space-time from the quadrupole and higher. It has been shown by Laarakkers & Poisson (1999) that while the Kerr quadrupole is equal to minus the square of the spin parameter, $q = -j^2$, where $q = M_2/M^3$, for realistic neutron stars the quadrupole becomes proportional to that of Kerr's with a proportionality constant greater than 1 and increasing with increasing stiffness of the EOS (it also decreases at higher masses). Similar behavior is observed for the spin octupole as well (discussed in Pappas & Apostolatos (2012)). From that perspective a Kerr black hole behaves as an object with a super-soft EOS.

Going further towards the inner regions of the disc (closer to the ISCO), the frequency of the vertical perturbation becomes greater than the orbital frequency up until the ISCO. This is evident in the plot of Ω_z/Ω versus Ω in the case of the L EOS [for the models of the sequence (i) of the corresponding neutron stars]. That effect would produce a distinctive behavior in the observed QPOs that could be used to select an equation of state, since whether or not such an effect is present or specifically the frequency range where one would expect to see it, depends on the stiffness of the EOS of the neutron star.

We can see similar behavior in the corresponding plots for the FPS and AU EOSs, with the difference that the vertical oscillation frequency does not always become greater than the orbital frequency before the ISCO is reached, as can be seen in Figs 2 and 3. The distinctive drop of the ratio Ω_z/Ω though remains.

In the plots we also indicate by a small triangle the surface of the star whenever it is at a radius that is further than the ISCO. Generally the ISCO is swallowed by the star for models of the first sequence for every EOS. For these models, the decrease of Ω_z/Ω is also more prominent, thus it becomes apparent even if the ISCO is swallowed by the star. As it can be seen for the case of L EOS, it might become negative even before reaching the star's surface.

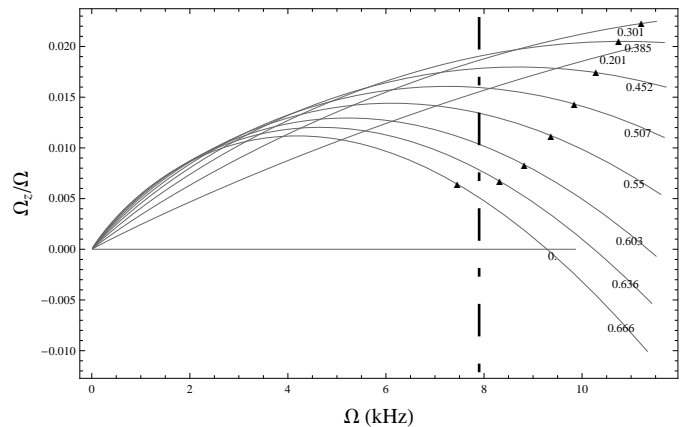


Figure 2. Ω_z/Ω as a function of Ω for the FPS EOS. The spin parameters $j = J/M^2$ are also indicated for every model.

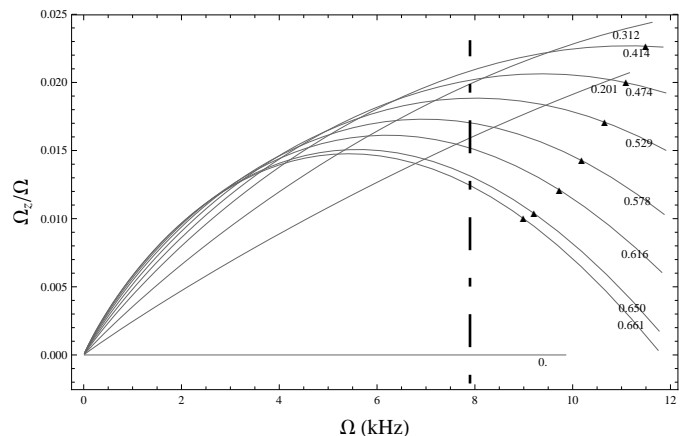


Figure 3. Same as Fig. 2 for the AU EOS.

Finally, a dashed-dotted line marks the position of the maximum measured QPO frequency ($\nu = 1258$ Hz) which corresponds to $\Omega \sim 7.9$ kHz. The plots show something that has been discussed in the literature, namely the fact that this particular frequency is incompatible with the L equation of state, since there is no model that could produce such a high frequency either because of the position of the ISCO or because of the position of the surface.

6 DISTINGUISHING DIFFERENT EQUATIONS OF STATE OF NEUTRON STARS

In this section, we will use the templates presented in the previous section and we will attempt to draw some conclusions about the EOS from observations. For illustrative purposes we will use observations from two sources as well, i.e., Scorpius X-1 (Sco X-1) represented by the filled squares and Circinus X-1 (Circ X-1) represented by the empty squares, as obtained from van der Klis et al. (1997) and Boutloukos et al. (2006).

Once we have the frequency templates for the various models that correspond to different EOSs, we can compare them to observations of the orbital frequency and of the periastron precession frequency, i.e., the twin kHz QPOs.

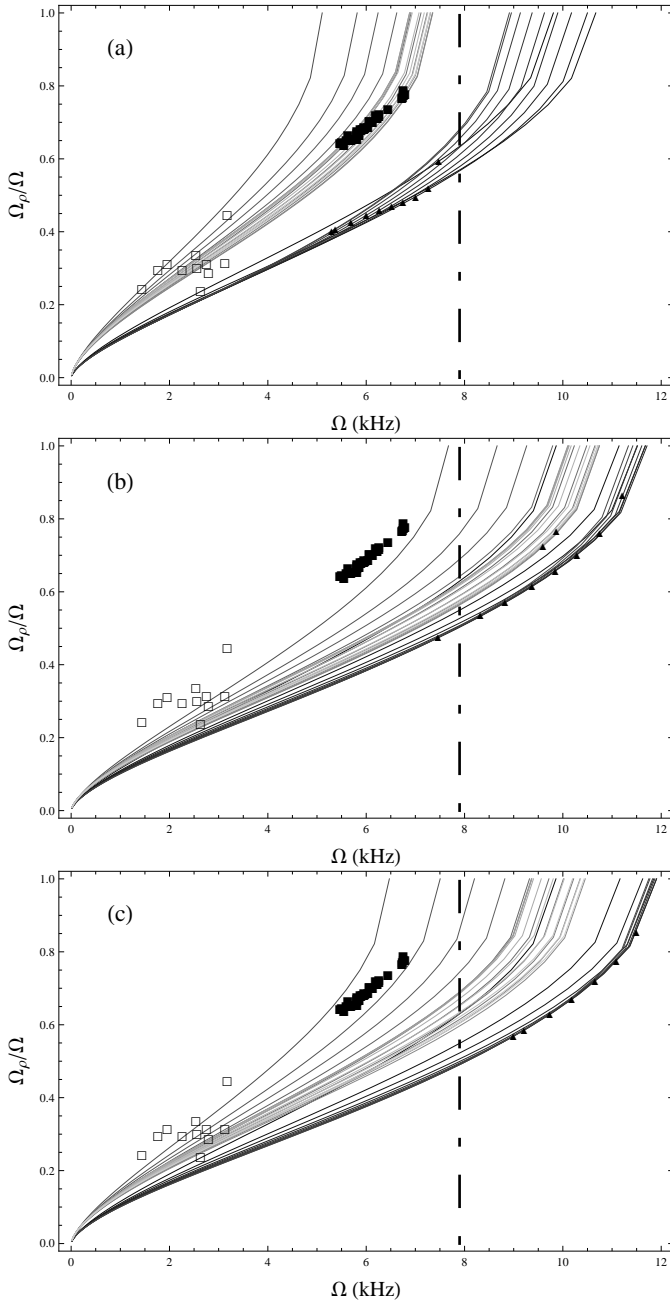


Figure 4. QPOs observations compared with the templates for the equations of state (a) L, (b) FPS, and (c) AU. The black triangles indicate the surface whenever it is present. The filled squares are observations related to the source Sco X-1 and the empty squares are observations of Circ X-1.

Such a comparison is shown in Fig. 4, where we have plotted the curves of Ω_ρ/Ω as a function of Ω for all the models of the three EOSs. The plots also show the observations of Sco X-1 and Circ X-1. An appropriate selection of observations of several sources compared with the frequency templates could select or exclude EOSs. For example the two sources shown here, appear not to fit very well with the FPS EOS. Furthermore, if one had good observations on one source, then one could select a specific model and thus estimate the mass and the spin of the neutron star, as well as its higher

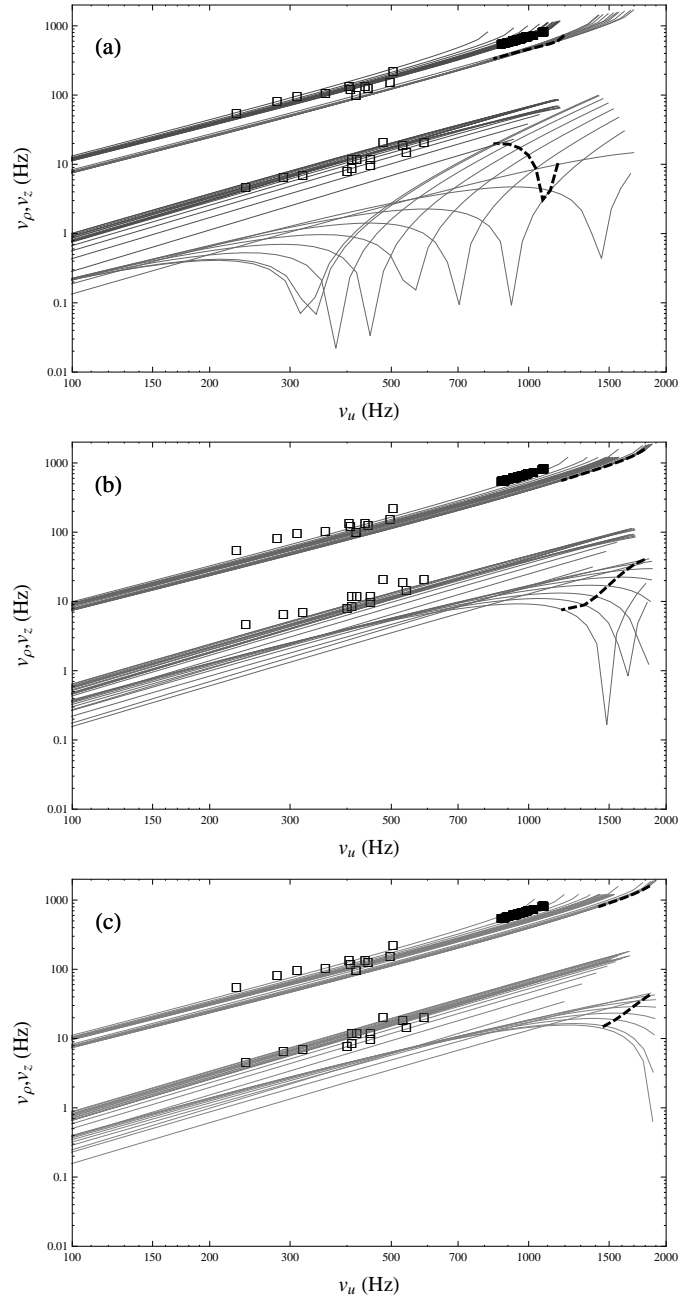


Figure 5. Simulated QPO frequencies related to the periastron and nodal precession (ν_ρ , ν_z) as functions of the orbital frequency (ν_u) for the models with equations of state (a) L, (b) FPS, and (c) AU. Since Ω_z could be either positive or negative, the ν_z is simply $|\Omega_z/2\pi|$. The characteristic features that appear on the nodal precession frequencies of the neutron stars do not appear in the corresponding frequencies for a Kerr background.

moments. That would offer the opportunity for investigating the interior structure of a neutron star.

In Fig. 5 we have plotted for the different EOSs what would be the observed frequencies ν of the various models, assuming that the upper kHz QPOs correspond to the orbital frequency, the lower kHz QPOs correspond to the periastron precession and the low-frequency QPOs correspond to the nodal precession. The plots also indicate with

a dashed curve the surface for the models that have their ISCO inside the star. This type of plots are often used to present data from various sources. For illustrative purposes we also show with black squares the kHz QPOs of Sco X-1 and with empty squares the kHz (upper grouping) and low-frequency (lower grouping) QPOs of Circ X-1. Although such a plot “masks” the differences of each source when we are considering kHz QPOs, it makes evident the behavior of the frequency of the nodal precession (low-frequency QPOs), that we discussed in the previous section. The turning of the low-frequency QPO to a horizontal path and the subsequent drop of the curve as the upper kHz QPO increases, that is evident in the L EOS plots, would be a clear signature that the observed frequencies are indeed related to orbital motions. The range of frequencies that such a behavior would be observed would also distinguish between different EOSs, as the three plots show, while with sufficient resolution one could identify a specific model from the frequency of that “drop”.

It should also be pointed out that the three different sequences of neutron star models that we have used group together in a similar fashion. The first sequence that corresponds to neutron stars that are not near the maximum stable mass at the non rotating limit ($M = 1.4M_{\odot}$) exhibits lower low-frequency QPOs that present the characteristic “drop” discussed previously, while the other two sequences (the one at the maximum stable mass in the non-rotating limit and the one with no stable non-rotating limit) group together to higher low-frequencies and do not show the aforementioned “drop”. Differences between the three sequences for the kHz QPOs are not that prominent, but depending on the EOS one could detect a small gap between the first sequence and the other two.

7 CONCLUSIONS

We have investigated the merits of applying some new tools in the study of compact objects from the observation of QPOs in the X-ray flux of accreting systems.

We have shown that Ryan’s asymptotic expressions for the frequencies, combined with the appropriate observations, can be useful in constraining the first three multipole moments of the compact object. That would offer us the opportunity to probe the structure of neutron stars, as well as the possibility of testing the validity of the no-hair theorem for black holes.

We have also demonstrated the potential benefits of using analytic space-times that are constructed so as to be faithful to the geometry around realistic neutron star models. The comparison of the observed QPOs to the ones calculated with such space-times, could potentially select or exclude EOSs for neutron stars or could even select specific neutron star models for specific sources. We have also shown that there are characteristic properties of the frequencies of the orbits in realistic neutron star space-times that the Kerr and Schwarzschild geometries cannot capture. Specifically the way that the nodal precession varies as one goes from lower to higher orbital frequencies would be a signature of the orbital nature for any observed QPOs that exhibit that behavior and could be used to distinguish different EOSs and probably even particular models of neutron stars.

Following this line of research it would be worth pursuing further, with the help of analytic space-times, the investigation of orbits that deviate significantly from the equatorial plane as well as the investigation of possible orbital resonances that can be observed for these space-times. The use of analytic instead of numerical geometries would greatly simplify such an exploration.

ACKNOWLEDGMENTS

I would like to thank Haris Apostolatos, Nektarios Vlahakis, Apostolos Mastichiadis, Kostas Glampedakis and Stratos Boutloukos for useful discussions. I would also like to thank Kostas Kokkotas for his hospitality at the Theoretical Astrophysics Section in Tübingen (TAT) and I thank Nikos Stergioulas for providing me access to his RNS numerical code. Finally, I would like to thank the anonymous referee for his/her comments and suggestions that helped improve on the clarity in the presentation of this work. This work has been supported by the IKY-DAAD programme (IKYDA 2010).

REFERENCES

- Berti E., Stergioulas N., 2004, MNRAS, 350 1416
- Boutloukos S., van der Klis M., Altamirano D., Klein-Wolt M., Wijnands R., Jonker P.G., Fender R.P., 2006, ApJ, 653, 1435
- Cook G.B., Shapiro S.L., Teukolsky S. A., 1994, ApJ, 424, 823
- Ernst F.J., 1968, Phys. Rev., 167, 1175
- Ernst F.J., 1968, Phys. Rev., 168, 1415
- Fodor G., Honselaers C., Perjés Z., 1989, J. Math. Phys., 30, 2252
- Geroch R., 1970, J. Math. Phys., 11, 2580
- Hansen R.O., 1974, J. Math. Phys., 15, 46
- Jonker P.G., in ‘t Zand J.J.M., Mendez M., van der Klis M., MNRAS, 378, 1187
- Krolik J.H., 1999, Active Galactic Nuclei: From the Central Black Hole to the Galactic Environment. Princeton Univ. Press, Princeton, NJ
- Laarakkers W.G., Poisson E., 1999, ApJ, 512, 282
- Lamb F.K., 2003, van den Heuvel E.P.J., Kaper L., Roi E., Wijers R.A.M.J., eds, ASP Conf.Ser. Vol. 308, From X-ray Binaries to Gamma-ray Bursts. Astron. Soc. Pac., San Francisco, p. 221
- Manko V.S., Sibgatullin N.R., 1993, Class. Quantum Grav., 10, 1383
- Manko V.S., Martin J., Ruiz J.E., 1995, J. Math. Phys., 36, 3063
- Pachón L.A., Rueda J.A., Sanabria-Gomez J.D., 2006, Phys. Rev. D, 73, 104038
- Papapetrou A., 1953, Ann. Phys., 12, 309
- Pappas G., 2009, J. Phys.: Conf. Ser., 189, 012028
- Pappas G., Apostolatos T.A., 2012, preprint (arXiv:gr-qc/1201.6067)
- Psaltis D., 2008, Living Rev. Relativ., 11, 9
- Rezzolla L., Yoshida S., Maccarone T.J., Zanotti O., 2003, MNRAS, 344, L37

- Ruiz E., Manko V.S., Martin J., 1995, *Phys. Rev. D*, 51, 4192
- Ryan F.D., 1995, *Phys. Rev. D*, 52, 5707
- Sibgatullin N.R., 1991, *Oscillations and Waves in Strong Gravitational and Electromagnetic Fields*. Springer, Berlin (original in Russian, 1984, Nauka, Moscow)
- Sotiriou T.P., Pappas G., 2005, *J. Phys.: Conf. Ser.*, 8, 23
- Stella L., 2001, in Malaguti G., Palumbo G., White N., eds, *AIP Conf. Proc. Vol. 599, X-ray Astronomy: Stellar Endpoints, AGN and the Diffuse Background*. Am. Inst. Phys., New York, p. 365
- Stergioulas N., 2003, *Living Rev. Relativ*, 6, 3
- Stergioulas N., Friedman J.L., 1995, *ApJ*, 444, 306
- Stute M., Camenzind M., 2002, *MNRAS*, 336, 831
- Teichmüller C., Fröb M.B., Maucher F., 2011, *Classical Quantum Gravity*, 28, 155015
- van der Klis M., 2006, in Lewis W.H.G., van der Klis M., eds, *Compact Stellar X-ray Sources*. Cambridge Univ. Press, Cambridge, p. 39
- van der Klis M., Wijnands R.A.D., Horne K., Chen W., 1997, *ApJ*, 481, L97